



Part-load performance modelling of a reheated humid air turbine power cycle



Giovanni D. Brighenti*, Pavlos K. Zachos*, Pau Lluís Orts-Gonzalez

Propulsion Engineering Centre, School of Aerospace, Transport and Manufacturing, Cranfield University, Cranfield MK43 0AL, Bedfordshire, United Kingdom

HIGHLIGHTS

- A novel method for the part-load performance simulation of a reheated HAT system is described.
- Predicted performance is shown across a range of turbine inlet temperatures settings.
- The impact of sea water and ambient air temperature on the performance of the cycle is evaluated.

ARTICLE INFO

Keywords:

Humid air turbine
Power generation
Part-load performance

ABSTRACT

Humid air turbines have previously demonstrated the potential to deliver high efficiency and power output combined with low emissions. This paper investigates the part-load performance of a 40 MW class advanced humid air turbine for power generation applications across a range of operating conditions. The paper investigates the impact of the main burner and reheater burner on the system's part-load power output and thermal efficiency and provides insights into the behavior of the key modules across the power spectrum of operation including the saturator tower which was never reported previously. The impact of the ambient air and sea water temperature on the cycle's performance are also investigated. The outcome of the research shows that the thermal efficiency if the system is less than 0.26% penalized when operating down to 50% of the design power output. Sea water temperature was found to have a more notable impact than ambient air temperature on both power output and thermal efficiency. Overall, this work constitutes a step ahead in understanding the potential benefits of an advanced humid air turbine system for power generation applications across a range of operating conditions which is not previously shown.

1. Introduction

Humid air turbine (HAT) systems are among the most efficient gas turbine based thermal cycles as highlighted by Jonsson and Yan in [1]. Previous studies (Rao et al. [2], Chiesa et al. [3], Jonsson and Yan [4]) have demonstrated effective utilization of low-quality waste heat within these cycles and the high thermal efficiency these systems can achieve. Chiesa et al. [3] performed a comparison between a number of humid cycles whereby HAT was identified as the most efficient, with a maximum thermal efficiency of 54%. Jonsson and Yan [5] and Traverso et al. [6] presented detailed techno-economic studies that showed that HAT cycles can offer lower investment cost and higher thermal efficiencies than combined gas turbine cycles (CCGT). Ågren and Westermarck [7,8] introduced the concept of saturator by-pass while Jonsson and Yan [5] proved that this would not only increase the efficiency of the cycles for high pressure ratios but also reduce the specific

investment cost of the whole system. Among others, Kavanagh and Parks ([9,10]), Moller et al. [11] and Nyberg et al. [12] studied the impact of each heat exchanger on the efficiency of the cycle. The influence of the ambient temperature on the off-design performance of the cycle was studied by Wang et al. [13] and Kim et al. [14] concluding that the cycle is less sensitive to ambient temperature variations than simple gas turbine cycles. Both works investigated the impact of the ambient temperature but since a closed water loop was assumed the impact of the water temperature was never considered. Wei et al. [15] conducted an experimental investigation on the off-design performance of a small-sized HAT cycle to conclude that the thermal efficiency increased by 3.1% compared to a simple cycle configuration. Takahashi [16] investigated the part-load performance of an advanced humid air turbine (AHAT) and the impact of ambient temperature. The off-design performance of the saturator tower was previously studied experimentally by Pedemonte et al. [17,18], whereas a methodology for the

* Corresponding authors.

E-mail addresses: g.d.brighenti@cranfield.ac.uk (G.D. Brighenti), p.zachos@cranfield.ac.uk (P.K. Zachos).

Nomenclature

Symbols

C	heat capacity (kJ/K)
C^*	heat capacity ratio (-)
kxA	overall heat transfer coefficient \times heat transfer area (Inverse of total resistance) (kW/K)
M	mass flow rate (kg/s)
P	pressure (MPa)
\dot{P}	power output (MW)
Q	heat transfer (MW)
R_a	specific gas constant of dry air (J/(kg K))
R_v	specific gas constant of dry vapor (J/(kg K))
T	temperature (K)

Abbreviations

AC	aftercooler
CC	combustion chamber
CCGTs	combined cycle gas turbines
CHAT	cascade humidified advanced turbine
EC	economizer
EvGT	evaporative gas turbine
HAT	humid air turbine
HPC	high-pressure compressor
HPT	high-pressure turbine
IC	intercooler

LPC	low-pressure compressor
LPT	low-pressure turbine
OPR	overall pressure ratio
pp	percentage point
PR	pressure ratio
PT	power turbine
REC	recuperator
RH	reheater
relPR	relative pressure ratio
SAT	saturator
TIT	turbine inlet temperature
vIGV	variable inlet guide vanes

Subscripts

a	dry air
g	gas
in	inlet
2	top section of the saturator
sat	saturation
w	water

Greek Symbols

β	saturator by-pass
ε	effectiveness
ω	absolute humidity
Φ	relative humidity

simulation of the saturator tower was developed by Aramayo-Prudencio et al. [19]. Brighenti et al. [20] studied the design point performance of a reheated humid air turbine cycle and the impact of the technology of selected components on the preliminary acquisition cost of the heat exchanger units. As Chiesa et al. [3] highlighted, such a cycle features notably better performance relatively to a single burner system that may promote the exploitation of humid cycle power plants in applications where high thermal efficiency and high power-to-plant size ratios are of importance.

A potential application for a reheated HAT system may be within the power generation or the marine propulsion markets. The high thermal efficiency and low NO_x and SO_x emissions [22] could potentially make such power plants attractive in view of future marine emission regulation [23]. Nevertheless, the part-load performance of open water loop HAT systems remains still unexplored. This paper presents a methodology for the modelling and simulation of the steady state part-load performance of a 40 MW reheated HAT cycle across a range of operating conditions. The impact of the outlet temperature of both combustion chambers on the power output and thermal efficiency of the cycle is examined. The impact of ambient air and water temperature on the cycle performance is also presented.

2. Methodology

2.1. Cycle description

Fig. 1 shows the reheated HAT cycle layout analyzed herein comprising a dual-shaft, and free power turbine gas-turbine arrangement. The cycle features a reheater combustion chamber upstream of the power turbine. A detailed description of the power system is presented by Brighenti et al. in [20]. In this study, an open water loop is used to supply the heat exchangers. The evaporation process in the saturator and an efficient droplet eliminator at the gas outlet of the saturator acts as a water-treatment device, enabling the use of direct sea water [24]. The cycle design is a result of the optimization of the design parameters

for maximum thermal efficiency as shown by Brighenti et al. [20]. No mechanical or heat losses are considered. The cycle design parameters is reported in Table 1.

To capture future trends in recuperator and air/water heat exchanger design and exploit the full thermal efficiency potential of the RHAT cycle, 90% recuperator effectiveness was assumed for this study while an effectiveness of 95% was assumed for all air/water heat exchangers. The assumed effectiveness level for the recuperator and the air/water heat exchangers is slightly higher than the current standards and as such larger units in size will be required with knock-on effects in the overall system's volume, weight and cost. The impact of the effectiveness (defined as $\varepsilon = Q/Q_{max}$) of the recuperator and air/water heat exchangers on the acquisition cost, weight and performance of the cycle layout at design point has been previously analyzed by Brighenti et al. in [20]. For the current study, the assumed heat exchanger effectiveness levels are considered to be representative of near future trends and are educated by the effectiveness levels of the WR21 heat exchangers previously reported by Crisalli and Parker in [21].

Marine diesel fuel proprieties were used for combustion calculations [25]. Turbine cooling flows are calculated using the methodology proposed by Young and Wilcock [26]. Typical values for maximum metal temperature ($T_{m,max} = 1300$ K), film cooling effectiveness

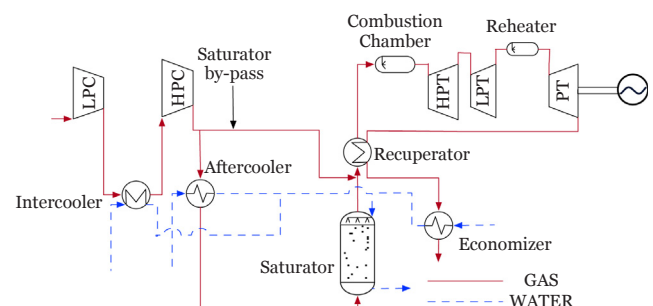


Fig. 1. Reheated HAT system layout.

Table 1
Cycle design parameters.

	Value	Constraints/assumptions
Ambient conditions		
Ambient temperature	288.15 K	
Ambient pressure	101.325 kPa	
Air relative humidity	80%	
Water temperature	288.15	
Compressors		
Overall pressure ratio	40:1	
Relative pressure ratio ($relPR = \log_{OPR} PR_{LPC}$)	0.526	$0.1 < relPR < 0.9$
Polytropic efficiency	90%	
Combustion chambers		
Combustion efficiency	99%	
Pressure loss	5%	
Turbine inlet temperature	1600 K	
Turbines		
High and low-pressure turbine polytropic efficiency	90%	
Power turbine polytropic efficiency	92%	
Recuperator		
Effectiveness	90%	
Hot-side pressure loss	5%	
Cold-side pressure loss	7.5%	
Air/Water heat exchangers		
Effectiveness	95%	
Inter-cooler water mass flow	15.4 kg/s	$C_{IC}^* = C_{min}/C_{max} \leq 0.95$ & $T_{w,out} \leq T_{sat} @ (0.9 * p_{SAT})$
After-cooler water mass flow	4.89 kg/s	$C_{AC}^* \leq 0.95$ & $T_{w,out} \leq T_{sat} @ (0.9 * p_{SAT})$
Economiser water mass flow	19.2 kg/s	$C_{AC}^* \leq 0.95$ & $T_{w,out} \leq T_{sat} @ (0.9 * p_{SAT})$
Pressure loss	7.5%	
Saturator		
Pinch temperature difference	5 K	
Pressure loss	5%	
Global parameters		
By-pass ratio $\beta = m_{g,SAT}/m_{g,GT \text{ inlet}}$	50.2%	$0\% \leq \beta \leq 100\%$
Gas inlet mass flow	40.89 kg/s	

($\epsilon_f = 40\%$) and internal flow cooling efficiency ($\eta_c = 70\%$) are assumed as discussed in [27]. The cooling flows are extracted downstream of the high-pressure compressor and upstream of the aftercooler.

2.2. Off-design modelling

The performance of the gas turbine and recuperator are resolved by TURBOMATCH [28,29] interfaced with MatLab functions for heat exchanger modelling. A Broyden based solver was employed to match the cycle components at part load [30]. The developed part load simulation algorithm is shown in Fig. 2. It requires the design point vector of the cycle and the off-design handles as free variables to control the engine operation. The system of checks and guesses used within TURBOMATCH as well as the integration of component maps within the scheme is further described by Pellegrini [29].

The performance model of the heat exchangers relies on the variation of the kxA coefficient foreach heat exchanging unit. Assuming that the flow properties of the two streams do not vary substantially from design point, Prandtl number and the thermal conductivity of the fluid can be considered fairly constant. Thus, the main driver for the variation of the heat transfer is the variation of the Reynolds number and consequently of the stream mass flow. The Dittu-Boelter heat transfer correlation, therefore, enables scaling of the kxA parameter at off-design conditions as:

$$kxA = kxA_{ref} \left(\frac{m_c^{0.8} m_h^{0.8}}{m_{c,ref}^{0.8} m_{h,ref}^{0.8}} \right) \left(\frac{m_c^{0.8} + m_h^{0.8}}{m_{c,ref}^{0.8} + m_{h,ref}^{0.8}} \right) \quad (1)$$

where c and h indicate the cold and hot streams and ref indicate the design values of the parameter.

The off-design effectiveness of the heat exchanger is calculated under the assumption that the flow arrangement can be approximated as being counter-current.

$$\epsilon = \frac{1 - \exp[-NTU(1-C^*)]}{1 - C^* \exp[-NTU(1-C^*)]} \quad (2)$$

where $NTU = kxA/C_{min}$ are the number of transfer units and $C^* = C_{min}/C_{max}$ is the heat capacity ratio between the two streams. Once the new effectiveness is defined, the outlet conditions of the heat exchanger are calculated with the definition of effectiveness as $\epsilon = Q/Q_{max}$. In order to avoid steaming within the heat exchanger, a threshold at the water outlet temperature is applied based on its saturation temperature at 90% of the pressure in the saturator:

$$T_{w,max} = T_{sat} @ (0.9 * p_{SAT}) \quad (3)$$

The pressure losses in each stream of the heat exchangers are calculated as suggested by Walsh and Fletcher in [30] as follows:

$$\frac{\Delta P}{P_{in}} = \alpha \left(\frac{m \sqrt{T_{in}}}{P_{in}} \right)^2 \quad (4)$$

where α is a pseudo loss coefficient derived at design point and remains constant at part-load calculations as discussed by Walsh and Fletcher in [31].

The model for the off-design performance calculations of the saturator is based on the Aramayo-Prudencio et al. [19] and Lindquist et al. [32]. The saturator's cross-section sizing is performed as shown by Dalili in [33] while the pressure drop across the device is estimated as shown by Coulson et al. in [34]. The model has been validated against experimental data from Lindquist et al. [32] as the maximum discrepancy is of 1.6% as reported by Brighenti et al. in [20].

3. Results and discussion

3.1. Impact of turbine inlet temperature

The $TITs$ of the main burner (TIT_{CC}) and reheater (TIT_{RH}) are used as handles for the part-load performance across the range reported in Table 2. The by-pass ratio of the saturator is kept constant at the design

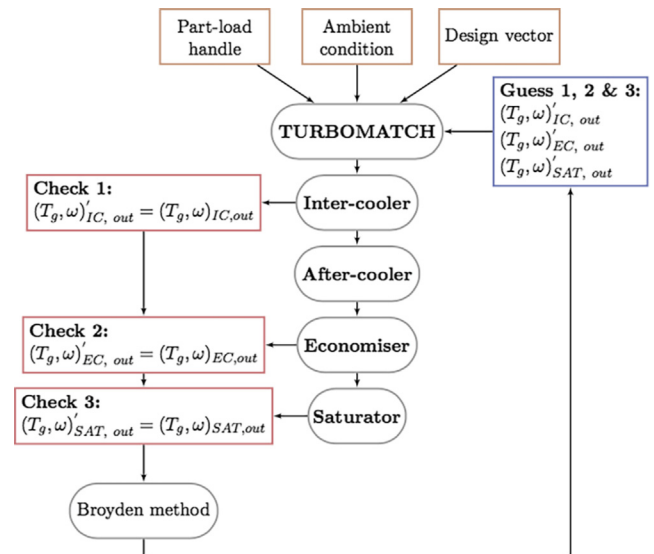


Fig. 2. Schematic layout of the Humid Air Turbine.

Table 2

Variation of the TIT of the main and reheater combustion chamber at part load.

TIT_{CC}	1600: – 25:1275 K
TIT_{RH}	1600: – 25:1200 K

value.

As long as no additional water is streamed into the heat exchangers to prevent steaming in the saturator, the water mass flow in each heat exchanger is kept constant at the design value. As such, the variation of the heat transfer coefficient of the heat exchanger (see Eq. (1)) becomes a function only of the gas mass flow.

Fig. 3 illustrates the system's running lines across a range of TIT_{CC} between 1600 K (design point) and 1275 K. The reduction in the turbine inlet temperature at the exit of the main burner (TIT_{CC}) results in a 65% reduction of inlet gas mass flow and a reduction in pressure ratio and non-dimensional mass flow at both compressors. The rotational speed of the low-pressure shaft is mostly affected by the reduction in TIT_{CC} from 1600 K to 1275 K and drops to 47% of the design value. For the same reduction in TIT_{CC} the rotational speed of the high-pressure shaft drops to 84% of the design value. Although typically a variation in the rotational speed between the two shafts is normal, this difference is further pronounced by the presence of the intercooler. Due to the presence of the intercooler, the temperature of the gas at inlet of the HPC drops by only 11 K when the TIT_{CC} is reduced from 1600 K to 1275 K which mitigates notable reductions in non-dimensional mass flow. The proximity of the operating point of the LPC to the surge line could raise issues related to the operability of the system in such conditions which will require special treatment of the compression system.

When TIT_{RH} is reduced from 1600 K to 1375 K and TIT_{CC} is kept constant at 1600 K (Fig. 4a–b) a 5.2% increase in the inlet flow of the cycle can be observed. The non-dimensional mass flow between the outlet of the LPT and the PT inlet increases due to the temperature rise in the reheater combustion chamber which, neglecting the fuel mass flow, it can be written as:

$$\left(\frac{m\sqrt{T}}{P}\right)_{PT,in} = \left(\frac{m\sqrt{T}}{P}\right)_{LPT,out} \sqrt{\frac{T_{PT,in}}{T_{LPT,out}}} \quad (5)$$

where $\sqrt{\frac{T_{PT,in}}{T_{LPT,out}}}$ is the temperature ratio across the reheater.

Given that the inlet non-dimensional mass flow does not vary significantly, the non-dimensional mass flow at the outlet of the LPT increases to satisfy Eq. (5) and the expansion ratio in the LPT also increases. This justifies the observed increase in the mass flow at the inlet of the gas turbine. This increase, nonetheless, depends on the variation of the humidity in the hot section of the cycle: if the humidity decreases, the increase in inlet gas mass flow is more significant than if the humidity remains constant or increases. Small variations in the pressure ratio of the high and low pressure compressors are observed as a result of the variations in the non-dimensional flow of the two systems.

Fig. 5 shows the thermal efficiency, power output and humidity at the inlet of the main burner of the HAT cycle across a range of main burner and reheater outlet temperatures. Two discrete regimes can be identified within the part load operating envelope of the cycle (A, B in Fig. 5a). Region A (Fig. 5a) where the system's power output is predominantly affected by the TIT of the main burner (TIT_{CC}), while the reduction in TIT_{RH} at constant TIT_{CC} is found to cause a slight increase the power output. In region B (Fig. 5a) although the TIT_{CC} remains the main driver of the power, a reduction in TIT_{RH} at constant TIT_{CC} causes a slight reduction in the power output. In terms of the system's thermal efficiency (Fig. 5b), there are again two discrete regions following the trend of the power output. Region A where the thermal efficiency is mainly dependent upon the TIT_{CC} and region B where the TIT_{RH} is found to have a detrimental effect on the efficiency of the cycle while

TIT_{CC} is only affecting it weakly.

The behavior of the system's power output across these identified part-load regimes A and B (see Fig. 5), is predominantly driven by the variations in gas humidity and temperature at the inlet of the combustion chamber as shown in Fig. 5c. Gas humidity (ω) depends on the pressure in the saturator tower (P_{SAT}), the relative gas humidity (Φ) and the air saturation pressure $P_{sat}(T_g)$ evaluated at the temperature of the gas T_g according to the following equation:

$$\omega = \frac{\Phi P_{sat}(T_g)}{P_{SAT} - \Phi P_{sat}(T_g)} \frac{R_a}{R_v} \quad (6)$$

Gas temperature (T_g) is in turn dependent upon the mass flows of the water and gas stream as well as upon the water inlet temperature at the saturation tower as described by Brighenti et al. in [20]. In region A of Fig. 5b the reduction in TIT_{CC} results in a reduction in humidity of the gas (Fig. 5c) that combined with the reduction in gas mass flow leads to a notable reduction in power output. Although the pressure in the saturator drops (Fig. 6a), the reduction in humidity is due to the water temperature drop at the inlet of the saturator (Fig. 6c) and a consequent drop in gas temperature at the top section of the saturator tower (Fig. 6b).

In region B TIT_{CC} has only a minor impact on the humidity reduction (Fig. 5c) as the water inlet temperature (Fig. 6c) in the saturator is less affected by TIT_{CC} than in region A. The smaller impact of the TIT_{CC} on the humidity leads to a weaker dependency of the power output

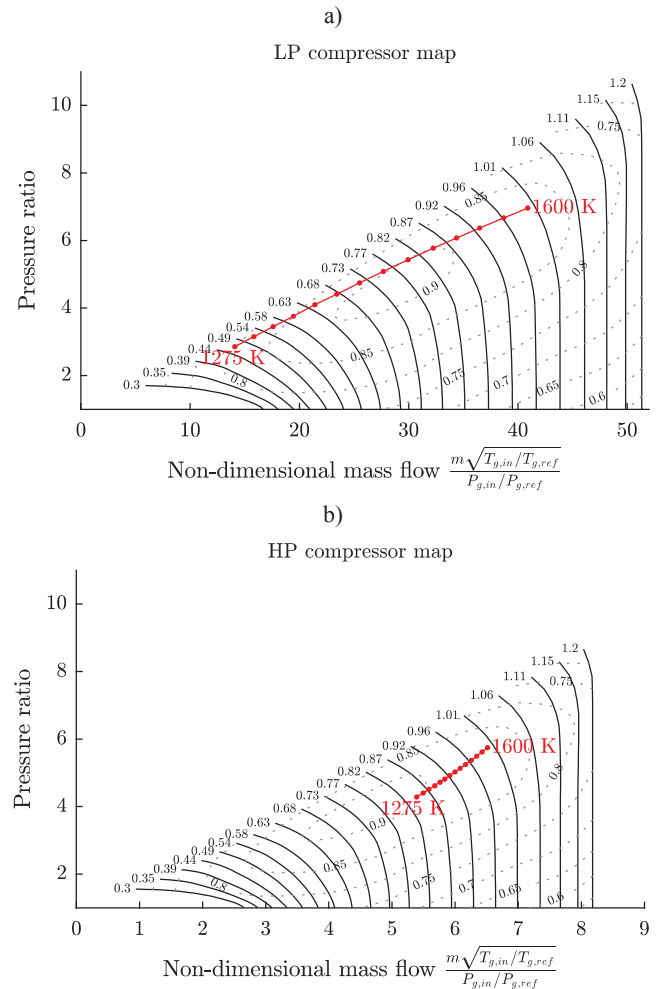


Fig. 3. Running lines with TIT_{CC} as a handle (in red) and $TIT_{RH} = 1600$ K. (a) low-pressure compressor and (b) high-pressure compressor map. (For interpretation of the references to color in this figure legend, the reader is referred to the web version of this article.)

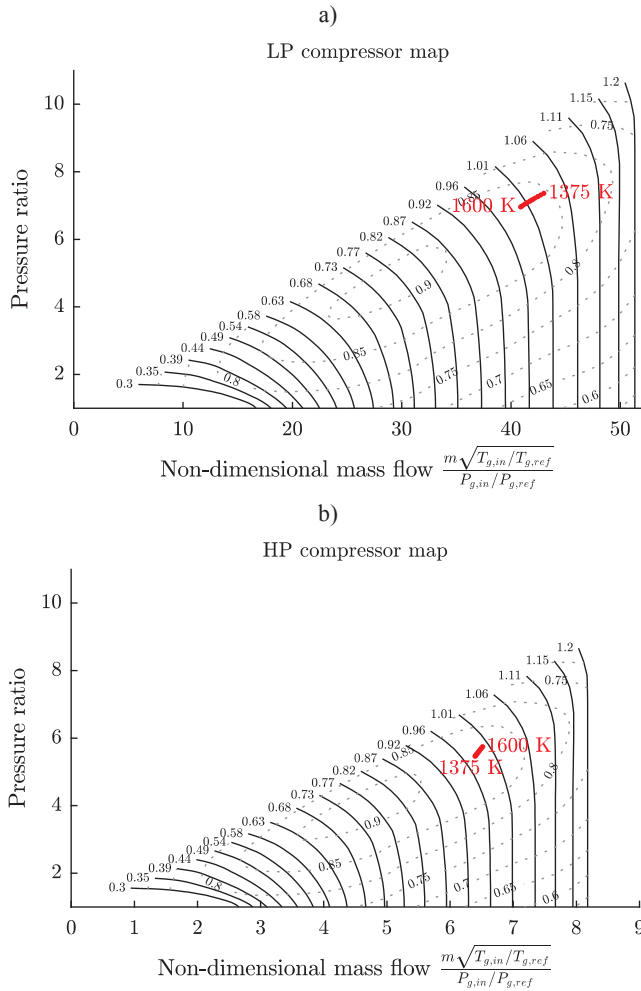


Fig. 4. Running lines with TIT_{RH} as a handle (in red) and $TIT_{CC} = 1600$. (a) low-pressure compressor and (b) high-pressure compressor map. (For interpretation of the references to color in this figure legend, the reader is referred to the web version of this article.)

upon the variations in TIT_{CC} . TIT_{RH} was found to have a more detrimental effect on the humidity of the gas in region B compared to region A (Fig. 5c). Although for reductions in TIT_{RH} the pressure in the saturator increases in both regions (A, B in Fig. 6a), the water

temperature (Fig. 6c) in region B drops whereas it increases across region A. The behavior of the water temperature at the inlet of the saturator is driven by the economizer performance within region A (see Eq. (3)). In region A the temperature of the water is directly affected by the pressure in the saturator, thus the temperature increases for reductions in TIT_{RH} . In region B, as the water to gas mass flow ratio is constant, the temperature is affected by the heat available in the economizer, thus the temperature drops for reductions in TIT_{RH} .

Cycle part-load control across a range of operating conditions is fundamental to maintain high thermal efficiencies across all power settings. Fig. 7a shows the variation of both power output and thermal efficiency across a range of TIT_{CC} and TIT_{RH} . The bold line with markers in Fig. 7a represents the operating points with maximum thermal efficiency for a power load between 100% and 25% of the design point power output. As shown in Fig. 7b, the highest thermal efficiency between 100% and 29% power output is achieved by a constant TIT_{RH} at its design value and a variable TIT_{CC} to control the load (Fig. 7b). Between 29% and 25% of power load a reduction in TIT_{RH} from 1600 K to 1500 K is also required as well as a reduction in TIT_{CC} to 1295 K. The efficiency of the cycle, between design point and 67% of power load, remains higher or equal to the design value, with a maximum increase of 0.16 pp at 80% of the power load. When at 50% of the power load, the thermal efficiency drops by 0.72 pp from the design value.

The cycle can be therefore operated down to approximately 50% of power load maintaining a thermal efficiency higher than 60%. Although the high thermal efficiency would limit the operating costs related to fuel consumption, the high TIT_{RH} needed across the power range to achieve such efficiencies may impact the life of the power turbine blade rows which may impact the maintenance costs. A full techno-economic analysis of the cycle for a specific operation would be necessary to assess the optimum part-load management of the cycle from a cost point of view.

An alternative common way for part-load control is via compressor variable inlet guide vanes (vIGVs). The performance of the reheated HAT cycle when varying the position of the vIGVs is studied by keeping the water to air mass flow ratio constant at the design values for all water to air heat exchangers. Both TIT_{RH} and TIT_{CC} are kept constant at 1600 K. Fig. 8 illustrates the impact of the vIGVs regulated inlet mass flow on the thermal efficiency and power output. When the cycle operates at 85% of the power output (34 MW) the thermal efficiency drops by 1.13 pp from the design point level. For the same power load of 34 MW, when achieved with the reduction of the TIT_{CC} , the thermal efficiency remains almost constant to the design point value (Fig. 7a). As such, operating the cycle at part load by using TIT_{CC} as handle,

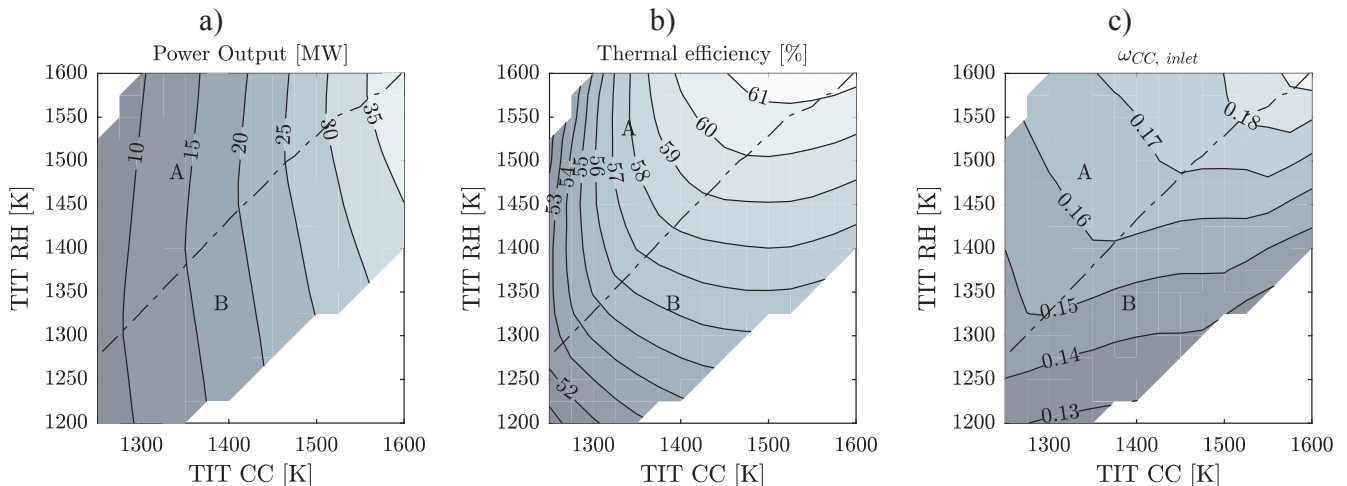


Fig. 5. Part-load performance of the HAT cycle across a range of main burner and reheater outlet temperatures. (a) power output, (b) thermal efficiency and (c) humidity at the inlet of the main burner.

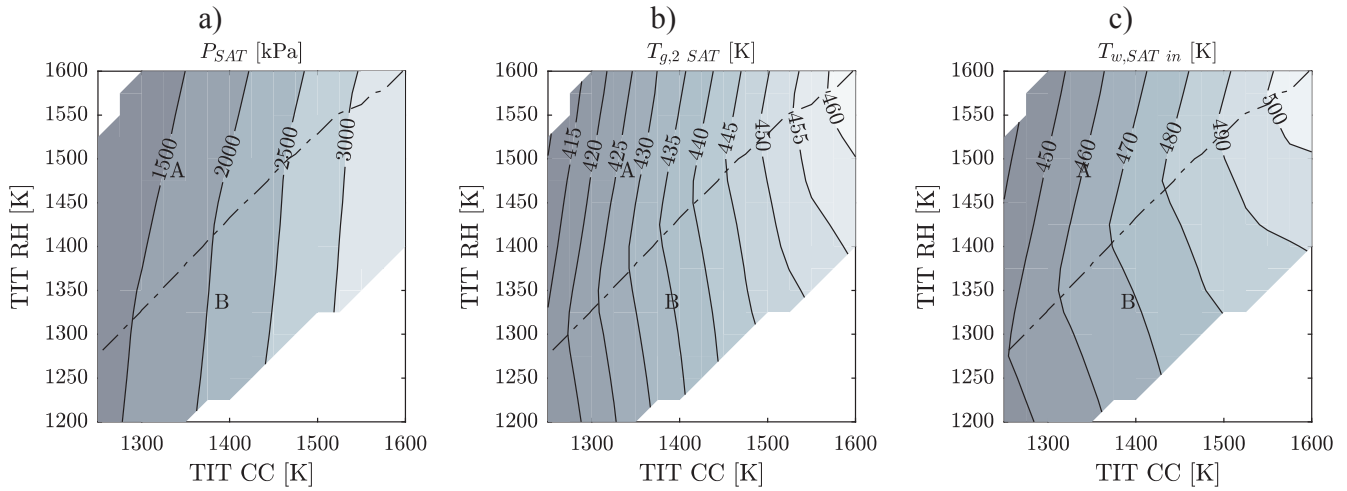


Fig. 6. (a) Saturator pressure, (b) gas outlet temperature and (c) water inlet temperature as a function of TIT_{CC} and TIT_{RH} .

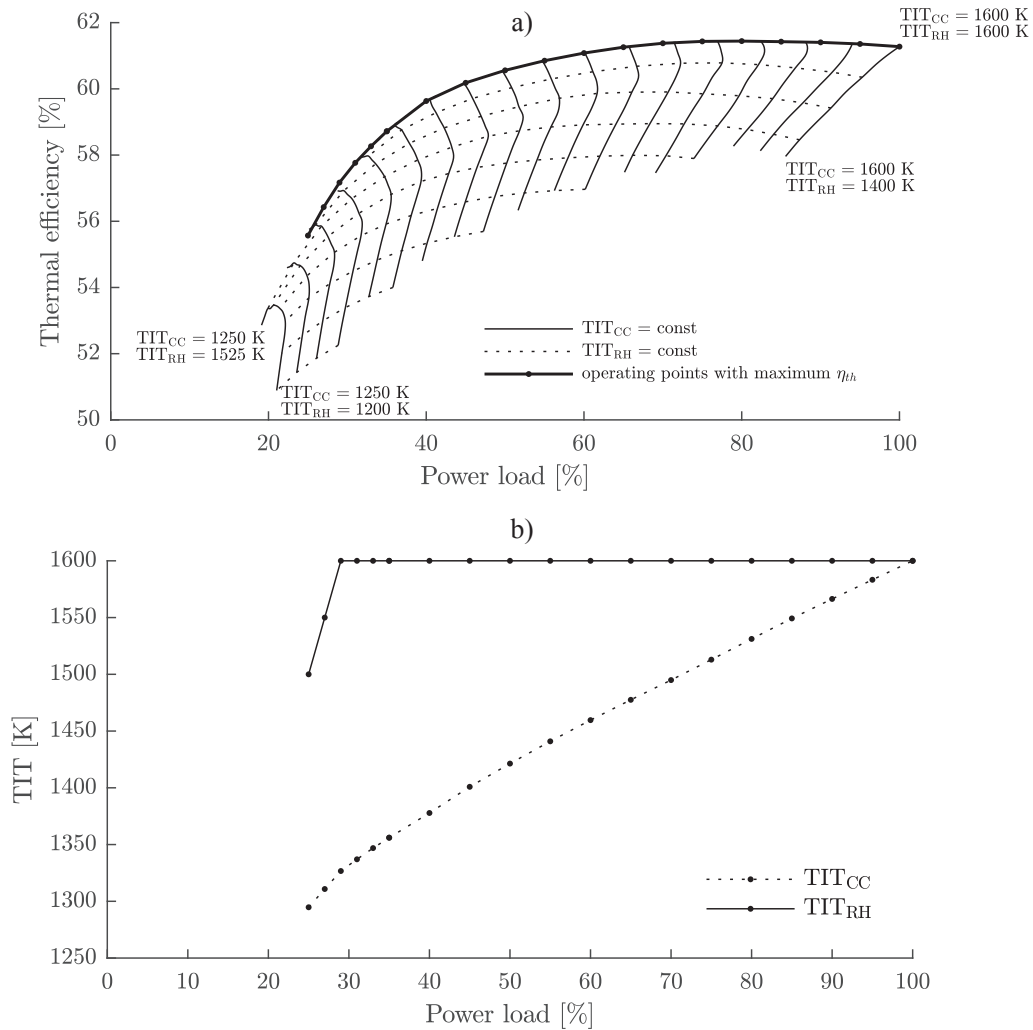


Fig. 7. (a) Thermal efficiency vs. power load in function of TIT_{CC} and TIT_{RH} . (b) TIT_{CC} and TIT_{RH} for maximum thermal efficiency across a range of power output.

rather the viGVs, seems a more viable approach from an efficiency prospective as well as from a maintenance cost viewpoint.

3.2. Impact of ambient conditions

In marine power applications, ambient air and sea water

temperature, in which such a power system can operate, can vary by several degrees depending on the time of day, season and latitude. The impact of ambient air and sea temperature on the cycle performance are studied at constant TIT_{CC} and TIT_{RH} at the nominal value of 1600 K. The water temperature (T_w) is varied parametrically from 280.15 K to 312.15 K whereas the ambient air temperature is varied as a function of

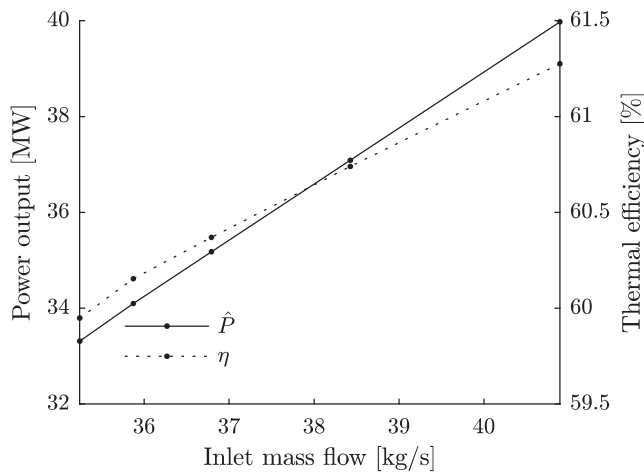


Fig. 8. Power output and thermal efficiency for performance control via vIGVs.

the water temperature from $T_w - 16$ K to $T_w + 16$ K. The water to air mass flow ratio is kept constant and if the temperature of the water at the outlet of the heat exchanger exceeds $T_{w,max} = T_{sat} @ (0.9 \cdot p_{SAT})$ then the water mass flow in that heat exchanger is increased so that $T_{HE,out} = T_{w,max}$.

Fig. 9 shows the variation in thermal efficiency and power output of the cycle as a function of water and air temperature. Thermal efficiency and power output are mostly affected by the ambient temperature for values higher than the design value of 288.15 K. The thermal efficiency and power output drop by 0.96 pp and 5.1 MW (12.7%) respectively for an increase in ambient temperature and sea water temperature of 10 K (308.15 K). Nevertheless, for the same air temperature (308.15 K), the variation of the water temperature from 292.15 K to 312.15 K penalises the thermal efficiency by 0.13 pp and the power output by 0.35 MW.

The reduction in power output and thermal efficiency is driven by the reduction in air compressibility for higher ambient temperatures and less effective inter-cooling for higher sea water temperature. In both cases, the new equilibrium steady state operating point of both HP and LP shafts shifts to lower power whereby gas mass flow (Fig. 10a) and pressure ratio are reduced. The humidity (Fig. 10b) on the other hand increases as a result of the reduction in pressure and the increase in water to air mass flow ratio in the saturator tower. This mitigates the reduction in power due to the reduction in compressibility of the air and pour inter-cooling compared to dry cycles. Part of the reduction in enthalpy available in the turbines due to the decrease in gas mass flow and pressure ratio is compensated by this increase in humidity.

For air temperatures below the design value the variations in thermal efficiency become very small. When both air and water temperatures decrease from the design values (288.15 K) to 280.15 K the thermal efficiency drops by only 0.09 pp whereas the power output

drops to 37.6 MW. In this region, where the air temperature is lower than the design value, the water temperature is found to have greater impact on power output than the air temperature (Fig. 9b).

Although previous research has shown that HAT cycles are able to achieve notably better performance in terms of thermal efficiency than combined steam-gas systems, the work presented herein identified potential shortcomings that may arise from the operation of such a system across a range of conditions which was never explored before. These are related to the operability of the compression system and the susceptibility this showed to the humidification across the operating envelop as well as with the impact of the ambient conditions on the cycle's performance and operability. In addition, humidified cycle technologies still present a number of unexplored areas which need addressing before any large scale deployment of such systems for power generation or propulsion applications. One of the main issues remains the volumetric mismatch in the flow rate between the compressors and turbines as a result of the enhanced humidification within the gas generator. Gas turbines able to accommodate the increased volumetric flow rate, necessary for the HAT to achieve its potential of high thermal efficiency, are yet to be developed. Moreover, HAT systems capable of achieving the high thermal efficiencies indicated in this work, will require the development of high effectiveness heat exchangers. Although the current trends in the heat exchanger market indicate that the required levels of effectiveness will be feasible in the near future, such technologies have yet to be fully demonstrated. At the moment, previous experience in operating heat exchangers as part of a gas turbine cycle for propulsion applications across a range of operating conditions is still limited to the WR-21 marine prime mover [21].

4. Conclusions

A study on the part-load performance of a reheated humid air turbine system is presented herein. The method developed to predict the stand-alone, off-design performance of key components including a validated method for the modelling of the saturator is shown. The integration of the individual models onto a system simulation platform is described. Key equations and iterative engine matching schemes are provided. The developed method was used for the system's performance analysis across a range of power settings in terms of turbine entry temperatures.

Variations in the turbine inlet temperature at the exit of both the main as well the reheater burners primarily affect the humidification process, which in turn drives the output power and thermal efficiency behavior across the range of operating conditions. Two discrete regimes were identified within the part load operating envelope of the cycle. In the first one, the variation in humidity injected into the cycle is driven by variation in the saturator's pressure. In this region the reduction of the TIT of both main and reheater burners results in a reduction in humidity. In the second region the variation in humidity levels is

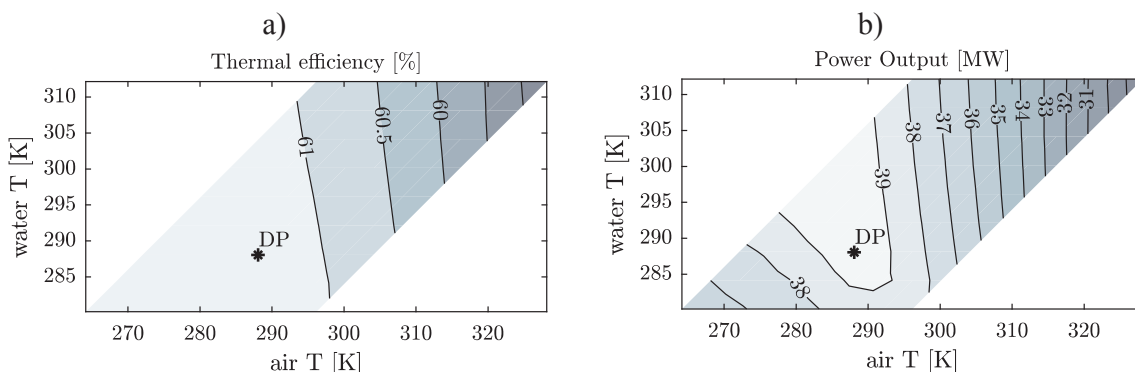


Fig. 9. (a) Thermal efficiency and (b) power output as a function of air and water temperature.

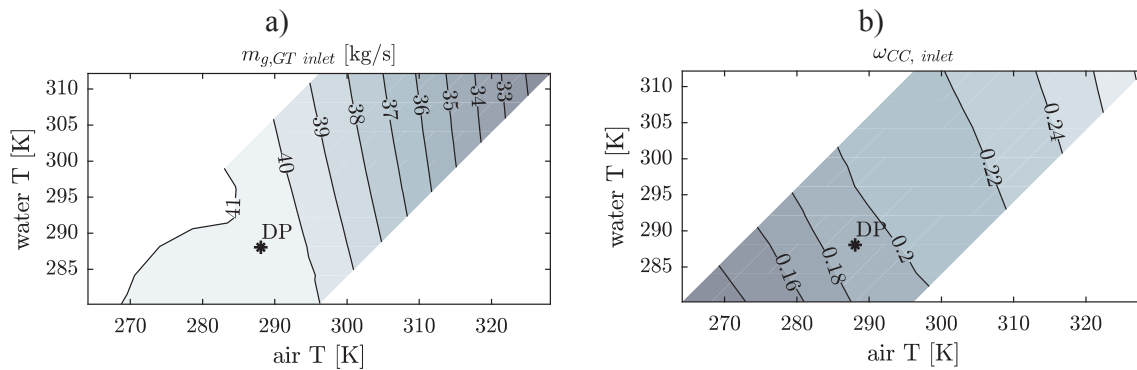


Fig. 10. (a) Gas mass flow and (b) humidity at the inlet of main burner as a function of the air and water temperature.

limited by the available heat in the air/water heat exchangers. In this region the reduction of the TIT of the main burner causes an increase in humidity, whereas the reduction of the TIT of the reheater burner results in a more notable reduction in humidity. The reheated HAT cycle was found able to achieve thermal efficiency beyond 55% across a wide range of power settings down to 25% of its design nominal power output with values above 60% across most of this range. Controlling the power output via the temperature at the exit of the reheater was found to have a detrimental effect on the system's thermal efficiency across the range of operation. Power output control via the main burner's exit temperature (TIT_{CC}) at constant reheater's temperature at its design value was found able to fully exploit the high thermal efficiency potential of the HAT system across the range of operation. However, varying the main burner's temperature (TIT_{CC}) was found to be associated with potential operability issues at the low pressure compression system as its surge margin can be notably penalized by the increase in pressure ratio. Operating point variations using variable geometry as part of the compression system may be able to mitigate some of the operability penalties observed across the range but was found to also have a detrimental effect on the cycle's efficiency at part load. Finally, the ambient air temperature was found to have a larger impact on the thermal efficiency and power output than the water temperature. Any variation in water and ambient air temperature from their design values was found to cause penalties to the power output of the system when the TIT at the outlet of both combustion chambers remains constant. The efficiency of the cycle was found unaffected by reductions in ambient air and water temperatures, whereas a reduction of approximately 0.1 pp per degree K was observed for higher than nominal ambient air temperatures driven by the amount of heat recuperated back into the cycle and the amount of heat and mass exchanged in the saturator tower.

Overall, the current work presents a novel methodology to enable performance predictions of a humid air turbine cycle across a range of operating conditions. The proposed method enables part load investigations of the reheated HAT system which were not previously possible with existing methods. A number of considerations with regards to the maturity of such system for the power generation market was also enabled. These are focused to the design and development of gas generator systems able to handle the notable volumetric discrepancy between the turbine and compression systems which is the result of the enhanced humidification in such a cycle but also on the availability of state of the art heat exchanging units able to deliver the effectiveness levels required to achieve high thermal efficiencies. The outcomes of this work constitute a step forward in understanding the behavior of a humid air turbine across a range of operating conditions and enable performance assessments even from the early stages of the preliminary design process.

Acknowledgments

This research program is financially supported by an EPSRC Industrial CASE Award and Rolls-Royce plc. under the University Technology Centre in Aero System Design, Integration and Performance at Cranfield University. The authors kindly thank Rolls-Royce plc. for permission to publish this work. Due to confidentiality agreements with research collaborators, supporting data can only be made available upon reasonable request and with permission of the industrial collaborator. For data requests please contact the corresponding author.

References

- [1] M. Jonsson, J. Yan, Humidified gas turbines—a review of proposed and implemented cycles, *Energy* 30 (7) (2005) 1013–1078.
- [2] A.D. Rao, V.J. Francuz, J.C. Shen, E.W. West, A Comparison of Humid Air Turbine (HAT) Cycle and Combined-Cycle Power Plants, EPRI, 1991.
- [3] P. Chiesa, G. Lozza, E. Macchi, S. Consonni, An assessment of the thermodynamic performance of mixed gas-steam cycles: Part B—water-injected and hat cycles, *J. Eng. Gas Turbines Power* 117 (Jul. 1995) 499–508.
- [4] M. Jonsson, J. Yan, Exergy analysis of part flow evaporative gas turbine cycles: Part 1—Introduction and method, in: Presented at the ASME Turbo Expo 2002: Power for Land, Sea, and Air, 2002, pp. 457–464.
- [5] M. Jonsson, J. Yan, Economic assessment of evaporative gas turbine cycles with optimized part flow humidification systems, in: Presented at the ASME Turbo Expo 2003: Power for Land, Sea, and Air, 2003.
- [6] A. Traverso, A.F. Massardo, Thermoeconomic analysis of mixed gas-steam cycles, *Appl. Thermal Eng.* 22 (2002) 1–21.
- [7] N.D. Ågren, M.O.J. Westermarck, Design study of part-flow evaporative gas turbine cycles: performance and equipment sizing—Part I: aeroderivative core, *J. Eng. Gas Turbines Power* 125 (1) (2003) 201–215.
- [8] N.D. Ågren, M.O.J. Westermarck, Design study of part-flow evaporative gas turbine cycles: performance and equipment sizing—Part II: industrial core, *J. Eng. Gas Turbines Power* 125 (1) (2003) 216–227.
- [9] R.M. Kavanagh, G.T. Parks, A systematic comparison and multi-objective optimization of humid power cycles—Part I: thermodynamics, *J. Eng. Gas Turbines Power* 131 (4) (Jul. 2009) 041701.
- [10] R.M. Kavanagh, G.T. Parks, A systematic comparison and multi-objective optimization of humid power cycles—Part II: economics, *J. Eng. Gas Turbines Power* 131 (4) (2009) 041702–041710.
- [11] B. F. Möller, M. Obana, M. Assadi, A. Mitakakis, Optimisation of HAT-cycles – with and without CO₂ capture, in: Presented at the ASME Turbo Expo 2004: Power for Land, Sea, and Air, 2004.
- [12] B. Nyberg, M. Thern, Thermodynamic studies of a HAT cycle and its components, *Appl. Energy* 89 (1) (2012) 315–321.
- [13] B. Wang, S. Zhang, Y. Xiao, Steady state off-design performance of humid air turbine cycle, in: Presented at the ASME Turbo Expo 2007: Power for Land, Sea, and Air, 2007.
- [14] T.S. Kim, C.H. Song, S.T. Ro, S.K. Kauh, Influence of ambient condition on thermodynamic performance of the humid air turbine cycle, *Energy* 25 (4) (Apr. 2000) 313–324.
- [15] C. Wei, S. Zang, Experimental investigation on the off-design performance of a small-sized humid air turbine cycle, *Appl. Thermal Eng.* 51 (1) (2013) 166–176.
- [16] T. Takahashi, Y. Nakao, E. Koda, Analysis and evaluation about advanced humid air turbine system, in: Presented at the Challenges on Power Engineering and Environment – Proceedings of the International Conference on Power Engineering 2007, ICOPE 2007, 2007.
- [17] A.A. Pedemonte, A. Traverso, A.F. Massardo, Experimental analysis of pressurised humidification tower for humid air gas turbine cycles. Part A: experimental campaign, *Appl. Thermal Eng.* 28 (14) (2008) 1711–1725.
- [18] A.A. Pedemonte, A. Traverso, A.F. Massardo, Experimental analysis of pressurised

- humidification tower for humid air gas turbine cycles. Part B: correlation of experimental data, *Appl. Thermal Eng.* 28 (13) (2008) 1623–1629.
- [19] A. Aramayo-Prudencio, J.B. Young, The analysis and design of saturators for power generation cycles: Part 2—heat and mass transfer, in: Presented at the ASME Turbo Expo 2003: Power for Land, Sea, and Air, 2003.
- [20] G. Brighenti, P. Orts-Gonzalez, L. Sanchez-de-Leon, P. Zachos, Design point performance and optimization of humid air turbine power plants, *Appl. Sci.* 7 (4) (2017) 413.
- [21] A.J. Crisalli, M.L. Parker, Overview of the WR-21 intercooled recuperated gas turbine engine system: a modern engine for a modern fleet, in: ASME 1993 International Gas Turbine and Aeroengine Congress and Exposition, May 1993.
- [22] T. Koganezawa, K. Miura, T. Saito, K. Abe, H. Inoue, Full scale testing of a cluster nozzle burner for the advanced humid air turbine, in: Presented at the ASME Turbo Expo 2007: Power for Land, Sea, and Air, 2007.
- [23] I. Marpol, Consolidated Edition 2006, MARPOL Annex VI: Regulations for the Prevention of Air Pollution from Ships, International Maritime Organization, London, 2006.
- [24] M. Bartlett, Developing Humidified Gas Turbine Cycles, Royal Institute of Technology, Stockholm, 2002.
- [25] E.M. Goodger, S.O.T. Ogaji, *Fuels and Combustion in Heat Engines*, Cranfield Design + Print, 2011.
- [26] J.B. Young, R.C. Wilcock, Modeling the air-cooled gas turbine: Part 2—coolant flows and losses, *J. Turbomach.* 124 (2) (2002) 214–218.
- [27] J.H. Horlock, D.T. Watson, T.V. Jones, Limitations on gas turbine performance imposed by large turbine cooling flows, *J. Eng. Gas Turbines Power* 123 (3) (2001) 487.
- [28] W.L. Macmillan, Development of a Module Type Computer Program for The Calculation of Gas Turbine Off Design Performance, Cranfield University, Cranfield, 1974.
- [29] A. Pellegrini, T. Nikolaidis, V. Pachidis, S. Köhler, On the performance simulation of inter-stage turbine reheat, *Appl. Thermal Eng.* 113 (Feb. 2017) 544–553.
- [30] C.G. Broyden, A class of methods for solving nonlinear simultaneous equations, *Math. Comp.* 19 (92) (1965) 577–577.
- [31] P.P. Walsh, P. Fletcher, *Gas Turbine Performance*, John Wiley & Sons, 2008.
- [32] T. Lindquist, M. Thern, T. Torisson, Experimental and theoretical results of a humidification tower in an evaporative gas turbine cycle pilot plant, in: Presented at the ASME Turbo Expo 2002: Power for Land, Sea, and Air, 2002.
- [33] F. Dalili, *Humidification in Evaporative Power Cycles*, Royal Institute of Technology, Stockholm, 2003.
- [34] J.F. Richardson, J.R. Backhurst, J.H. Harker, J.M. Coulson, Coulson and Richardson's Chemical Engineering, Particle Technology and Separation Processes, vol. 2, Butterworth Heinemann, Oxford, 2002.

2018-04-11

Part-load performance modelling of a reheated humid air turbine power cycle

Brighenti, Giovanni D.

Elsevier

Brighenti GD, Zachos PK, Orts-Gonzalez PL. (2018) Part-load performance modelling of a reheated humid air turbine power cycle. *Applied Thermal Engineering*, Volume 138, June 2018, pp. 365-373

<https://doi.org/10.1016/j.applthermaleng.2018.04.056>

Downloaded from Cranfield Library Services E-Repository